



## UvA-DARE (Digital Academic Repository)

### Building tools for image-guided adaptive radiotherapy of bladder cancer

Chai, X.

**Publication date**  
2012

[Link to publication](#)

#### **Citation for published version (APA):**

Chai, X. (2012). *Building tools for image-guided adaptive radiotherapy of bladder cancer*. [Thesis, fully internal, Universiteit van Amsterdam]. Boxpress.

#### **General rights**

It is not permitted to download or to forward/distribute the text or part of it without the consent of the author(s) and/or copyright holder(s), other than for strictly personal, individual use, unless the work is under an open content license (like Creative Commons).

#### **Disclaimer/Complaints regulations**

If you believe that digital publication of certain material infringes any of your rights or (privacy) interests, please let the Library know, stating your reasons. In case of a legitimate complaint, the Library will make the material inaccessible and/or remove it from the website. Please Ask the Library: <https://uba.uva.nl/en/contact>, or a letter to: Library of the University of Amsterdam, Secretariat, P.O. Box 19185, 1000 GD Amsterdam, The Netherlands. You will be contacted as soon as possible.

# Chapter 5

## **Automatic bladder segmentation on CBCT for multiple plan ART of bladder cancer using a patient-specific bladder model**

Xiangfei Chai, Marcel van Herk, Anja Betgen, Maarten Hulshof and Arjan Bel

*Physics in Medicine and Biology, 2012 (In press)*

## **Abstract**

**Purpose:** In multiple plan adaptive radiotherapy (ART) strategies of bladder cancer, a library of plans corresponding to different bladder volumes is created based on images acquired in early treatment sessions. Subsequently, the plan for the smallest PTV safely covering the bladder on cone-beam CT (CBCT) is selected as the plan of the day. The aim of this study is to develop an automatic bladder segmentation approach suitable for CBCT scans and test its ability to select the appropriate plan from the library of plans for such an ART procedure.

**Material and methods:** Twenty-three bladder cancer patients with a planning CT and on average 11.6 CBCT scans were included in our study. For each patient, all CBCT scans were matched to the planning CT on bony anatomy. Bladder contours were manually delineated for each planning CT (for model building) and CBCT (for model building and validation). The automatic segmentation method consisted of two steps. A patient-specific bladder deformation model was built from the training data set of each patient (the planning CT and the first 5 CBCT scans). Then, the model was applied to automatically segment bladders in the validation data of the same patient (the remaining CBCT scans). Principal component analysis (PCA) was applied to the training data to model patient-specific bladder deformation patterns. The number of PCA modes for each patient was chosen such that the bladder shapes in the training set could be represented by such number of PCA modes with less than 0.1 cm mean residual error. The automatic segmentation started from the bladder shape of a reference CBCT, which was adjusted by changing the weight of each PCA mode. As a result, the segmentation contour was deformed consistently with the training set to fit the bladder in the validation image. A cost function was defined by the absolute difference between the directional gradient field of reference CBCT sampled on the corresponding bladder contour and the directional gradient field of validation CBCT sampled on the segmentation contour candidate. The cost function measured the goodness of fit of the segmentation on the validation image and was minimized using a simplex optimizer. For each validation CBCT image, the segmentations were done five times using a different reference CBCT. The one with the lowest cost function was selected as the final bladder segmentation. Volume and distance based metrics and the accuracy of plan selection were evaluated to quantify the performance.

**Results:** Two to four PCA modes were needed to represent the bladder shape variation with less than 0.1 cm average residual error for the training data of each patient. The automatically segmented bladders had a 78.5% mean conformity index with the manual delineations. The mean SD of the local residual error over all patients was 0.24 cm. The agreement of plan selection between automatic and manual bladder segmentations was 77.5%.

**Conclusion:** PCA is an efficient method to describe patient-specific bladder deformation. The statistical shape based segmentation approach is robust to handle the relatively poor CBCT image quality and allows for fast and reliable automatic segmentation of the bladder on CBCT for selecting the appropriate plan from a library of plans.

## 5.1 Introduction

Modern radiotherapy (RT) techniques allow for planning and delivery of complex dose distributions that increase the dose to target volumes with better sparing of normal tissue. However, anatomical changes in patients limit the benefits of these techniques. The bladder is an example of a target organ that significantly varies in size and position during the course of fractionated radiotherapy [15;18]. Large isotropic margins of 1.5 to 2 cm are routinely used around the entire bladder target to compensate for this geometrical uncertainty, although in some cases these margins will still be inadequate [18;54]. This large geometrical uncertainty of the bladder considerably limits the radiation dose and result in large amounts of normal tissue (small bowel and rectum) receiving the same dose as the target.

Adaptive radiotherapy (ART) is becoming an important option for bladder cancer treatment as it enables a correction of deformation of the target by re-optimizing the plan during the course of the treatment [53]. Traditionally ART is an offline strategy, where after reviewing serial repeat scans, a new plan is made to correct the systematic errors [26;54].

Recently, various groups have developed multiple plan ART strategies for bladder cancer [22;23;29;55-58]. In such treatment strategies, multiple plans with different bladder volumes are created offline based on images acquired before or early during treatment. Subsequently, the plan for the smallest PTV safely covering the bladder on CBCT is selected online as the plan of the day. All reported that the multiple plan ART improves coverage of the bladder CTV and/or reduces the amount of small bowel irradiated, compared to the offline adaptive plan or traditional planning [22;23;29;54-57].

However, multiple plan ART is difficult to implement because complex decision making must take place at the treatment console immediately before treatment with the patient on the couch. In practice, after the daily CBCT scanning just before treatment, 95% isodose contours of multiple plans are overlaid on top of the CBCT images and the plan can be manually shifted to correct for deformation and displacement of bladder. Bladder coverage is visually assessed and the smallest PTV, in which the 95% isodose contour safely covers the bladder on CBCT, is selected as the plan of day. Given the poor soft-tissue contrast of CBCT, the border of the bladder on CBCT is, however, not always clearly visible. Therefore, plan selection is tedious in practice. Burrige et al. reported that the intra-subject and inter-subject agreement of plan selection are 73% and 70%, respectively [55]. Lalondrelle et al. found that different observers choose the same plan 76% of the time, and that the plan selection and assessment take on average 1.5 and 2.5 minutes, respectively [23]. One possible approach to improve plan selection consistency is a training program [116]. Foroudi et al. reported that after 11 hours of training, the agreement of plan selection increased from 72.7% to 87.9% [116].

To facilitate the clinical implementation of multiple plan ART of bladder cancer, automatic bladder segmentation on CBCT is therefore highly desired for making a faster and more accurate plan selection. However, due to the artifacts, e.g. ring, cupping and streak artifacts, and poor soft-tissue contrast of CBCT, simple intensity

or gradient based segmentation methods, e.g. threshold, snakes or level-set segmentation, usually fail to segment the bladder on CBCT.

Several groups developed deformable model based 3D bladder segmentation methods [117-119]. These methods all can simultaneously segment multiple male pelvic structures and yield good results on bladder segmentation on CT. However, these methods were developed for planning CT and their abilities on CBCT were not reported. Price et al. [120] proposed a semi-automatic method of bladder segmentation on CBCT that combines user defined support points on the visible bladder edge and a statistical bladder model to segment bladder on CBCT. Lu et al. [121] involved a statistical model and non-rigid registration to automatically segment bladder, prostate and rectum on CBCT. Both studies have small validation data set.

In this paper, we developed a novel automatic bladder segmentation method using patient-specific bladder shape information and applied it to a large patient group. For each patient, a principal component analysis (PCA) based statistical model is built to estimate the patient-specific bladder shape variation from the planning CT and the first five CBCT scans acquired early during treatment. The same scans can be used to generate multiple plans in the ART protocol.

The aim of this study is to present this automatic bladder segmentation approach and test its ability to select the appropriate plan from the library of plans for a multiple plan ART procedure.

## **5.2 Materials**

### **5.2.1 Patients**

From October 2003 to July 2006, 43 bladder cancer patients were treated with radiotherapy under CBCT guidance at the Department of Radiation Oncology of the Netherlands Cancer Institute / Antoni van Leeuwenhoek Hospital. They all had T2 to T4 N0M0 muscle invasive bladder tumors. Only 23 (3 female, 20 male) of the 43 patients were included in this study. The remaining 20 patients were excluded due to the following reasons: (1) lipiodol markers were injected into the bladder wall (9 patients); (2) urinary catheter was inserted during treatment (1 patient); (3) less than six CBCT scans (2 patients); (4) image quality of CBCT scans is not good enough for manual bladder delineation (2 patients) and (5) CBCT data is missing due to technical reasons (6 patients).

Fourteen out of the 23 included patients received partial bladder treatment with full bladder protocol and the remaining 9 patients received whole bladder treatment with empty bladder protocol. For the full bladder protocol, patients were instructed to void, drink 250 ml of water, and refrain from urination at least 1.5 hours before simulation and treatment. For the empty bladder protocol, patients were instructed to empty their bladder before simulation and treatment.

The CBCT data used in this study were all acquired before 2007, because a marker-based guidance procedure was introduced later [81], which is incompatible with our proposed segmentation procedure.

### **5.2.2 Image data and delineations**

Each patient received one planning CT scan and 7-20 (average 11.6) CBCT scans. The first 5 CBCT scans were acquired just before radiation delivery while the other CBCT scans were acquired before or both before and after radiation delivery on a CBCT-IGRT system (Elekta Synergy). The resolution of the CBCT scans are either  $256*256*256$  or  $400*400*120$ , with a voxel size of  $1.0*1.0*1.0$  mm<sup>3</sup>. The acquisition parameters of the projection images for CBCT scans were either 130 kV, 32 mA, 40 ms per projection or 130 kV, 80 mA, 20 ms per projection. 256 projection images were acquired for each CBCT reconstruction.

All CBCT scans were matched to the planning CT on bony anatomy. The bladder contours of all CT and CBCT scans were manually delineated slice-by-slice by two observers. For each patient, the bladder contours of the planning CT and the first five CBCT scans were used to construct a patient-specific statistical bladder model. The bladder contours of the rest of the CBCT scans were used to validate the segmentation algorithm.

## **5.3 Methods**

Our method consists of two parts: an offline training process where a statistical bladder model was built to extract a patient-specific bladder deformation pattern from existing bladder contours in CBCT images acquired early during treatment and an online 3D bladder segmentation process in which this patient-specific bladder model was applied to segment the bladder on validation CBCT images.

### **5.3.1 Training process**

#### **5.3.1.1 Parameterization of bladder geometry**

For each patient, six bladder contours were included in the patient-specific training data set. The slice-by-slice delineated bladder contours were converted to a 3D surface mesh consisting of vertices and triangular connections. The 3D surface mesh was smoothed with three iterations to eliminate unnatural shape differences between different slices. This surface smoothing algorithm is a simple umbrella operator, in which each vertex is moved to the average position in space of all its neighboring vertices [122]. The volume shrinkage effect caused by smoothing is compensated afterwards by scaling to the same volume as the original one.

The six bladder contours were aligned after matching all five CBCT images with the planning CT based on bony anatomy (figure 5.1). A reference point was set at 3 cm cranial and 3 cm posterior the center of the pubis bone for male, and at 2 cm cranial and 3 cm posterior from the center of the pubis bone for female, since the female bladder is in a lower position than male bladder. The reference positioning is similar to the reference point defined by Lotz et al. [40]. For some patients with very small bladder volumes, this reference point was manually adjusted to ensure it was situated inside all six bladder contours of a particular patient and that the entire surface of each bladder could be “seen” from this point. As long as the reference point was located inside the contours, the segmentation was not sensitive to the location of the reference point. A uniform 3D sphere contour with 2091 evenly distributed vertices was created and centered on the defined reference point. The six bladder contours were then re-sampled in 3D at the intersection of the 2091 radial lines passing through the reference point and bladder contours (figure 5.2). 2091 was an arbitrary number and the 2091 re-sampling lines in radial directions were considered to be dense enough to fully capture the feature points of bladder surface.

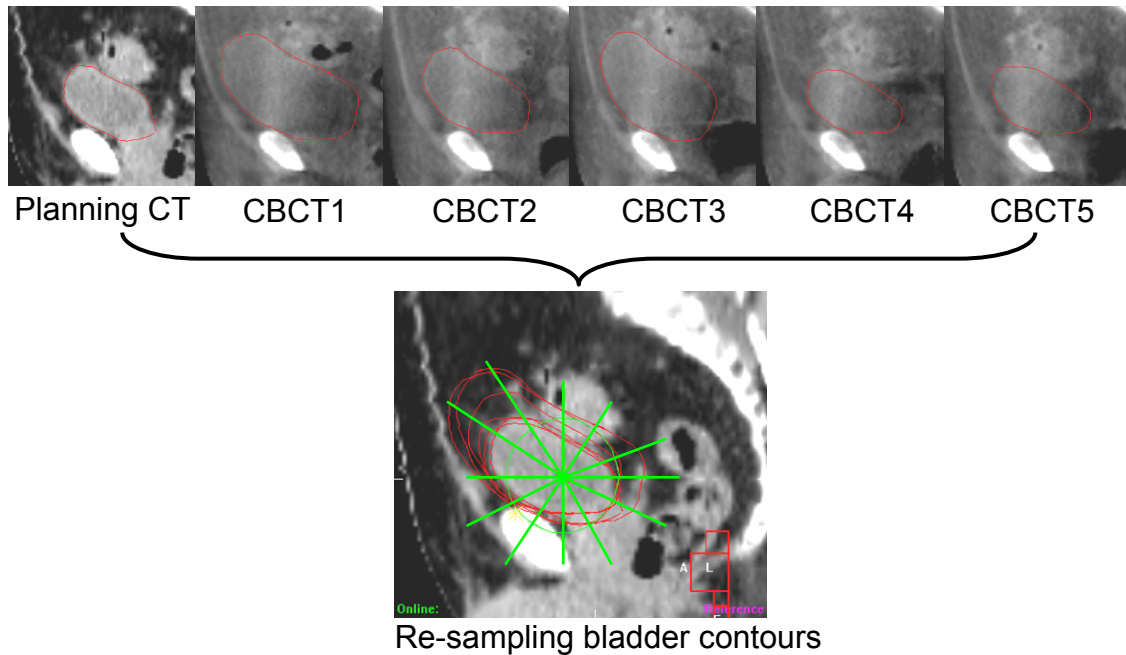


**Figure 5.1:** The first five CBCT scans were aligned to the planning CT by bony registration and displayed in a sagittal direction. The surfaces of the six bladder contours were all re-sampled radial from a reference point. Vertices in different contours with same angle relative to reference point were considered as corresponding points for PCA modeling.

After re-sampling, each bladder shape in the training data set was parameterized by a set of  $L$  ( $L = 2091$ ) vertices. If  $\overline{x}_j(i)$  denoted the position of  $j$ th vertex ( $j=1, \dots, 2091$ ) in the  $i$ th bladder contour, then the  $i$ th bladder geometry in the training dataset could be represented by the shape vector  $\mathbf{p}_i$  with dimensions  $3L$ .

The vertices from different bladder contours re-sampled by the same radial lines were considered as corresponding points in the PCA procedure, i.e., the series of

corresponding positions  $\vec{x}_j(1), \dots, \vec{x}_j(N)$  ( $N = 6$ ) provides point-tracking information on the six bladder contours.

### 5.3.1.2 Statistical model of bladder shape change based on PCA

It was assumed that the set of surface shape vector  $\{\mathbf{p}_i\}_{i=1,\dots,N}$  could be seen as samples from a random process. For anatomical reasons, displacements of  $L$  vertices due to bladder deformation were highly correlated, which implied that the dimensionality of the multivariate statistical problem was actually much smaller than  $3L$ . For a  $3L$  dimensional problem with  $N$  samples, we used a method from multivariate statistics, principal component analysis (PCA) [83;123], to model the anatomical bladder shape variation.

The bladder surface shape vectors were decomposed into eigenmodes. From the  $\mathbf{p}_i$  vectors, the mean shape vector  $\mathbf{p}_0$  was first computed:

$$\mathbf{p}_0 = \frac{1}{N} \sum_{i=1}^N \mathbf{p}_i \quad (5.1)$$

and the variation of the shape was summarized in the covariance matrix  $\mathbf{C}$  with dimensions  $3L \times 3L$

$$\mathbf{C} = \frac{1}{N-1} \sum_{i=1}^N (\mathbf{p}_i - \mathbf{p}_0) \cdot (\mathbf{p}_i - \mathbf{p}_0)^T \quad (5.2)$$

The shapes of the deformed organ were next decomposed by a mean shape and a weighted sum of  $N$  eigenmodes:

$$\mathbf{p} = \mathbf{p}_0 + \sum_{n=1}^N \psi_n \mathbf{q}_n, \quad \|\mathbf{q}_n\| = 1 \quad (5.3)$$

where the vectors  $\mathbf{q}_n$  were the eigenvectors of matrix  $\mathbf{C}$ , corresponding to the  $N$  eigenvalues  $\lambda_n$ . The coefficients  $\psi_n$  were normally distributed random variables with zero mean and variances  $\lambda_n$ .

Using only  $D$  ( $D < N$ ) eigenmodes, we reconstructed a new shape vector  $\mathbf{p}^{[D]}$  which was similar to the original shape vector  $\mathbf{p}$ .

$$\mathbf{p}^{[D]} = \mathbf{p}_0 + \sum_{n=1}^D \psi_n \mathbf{q}_n, \quad \|\mathbf{q}_n\| = 1 \quad (5.4)$$

The capability of the chosen  $D$  eigenmodes to represent the bladder shape in the training set was measured by calculating the difference  $\mathbf{e}^{[D]}$

$$\mathbf{e}^{[D]} = \mathbf{p}^{[D]} - \mathbf{p} \quad (5.5)$$

$\mathbf{e}_{i,j}^{[D]}$  is the 3D vector of local representation error of  $j$ th vertex and  $i$ th contour.

The mean residual error overall  $L$  vertex of  $N$  contours is

$$\mathbf{R}^{[D]} = \frac{1}{N} \sum_{i=1}^N \left( \frac{1}{L} \sum_{j=1}^L \|\mathbf{e}_{i,j}^{[D]}\| \right) \quad (5.6)$$

where  $\|e_{i,j}^{[D]}\|$  is the vector length of 3D vector  $e_{i,j}^{[D]}$ .

When  $D=N$ , ( $N=6$ ), the original shape matrix can be fully reconstructed and the overall mean residual  $R^{[D]}$  is 0.

The idea now is that using a small number  $D$ , the  $N$  vector  $p_i$  can be approximately represented by  $p_0$  and few PCA modes, characterized by  $D$  vectors  $q_n$  and  $D$  scalars  $\lambda_n$ . The number of eigenmodes  $D$  for each patient was chosen such that the mean residual  $R^{[D]}$  over six training contours was smaller than the voxel size (1 mm). The  $D$  eigenmodes were used to guide the segmentation of bladder on the online localization CBCT image.

### 5.3.2 Bladder segmentation guided by statistical bladder model

The bladder segmentation on online CBCT images was done based on the following two assumptions. First, the bladder shape variation observed in the first six scans was considered representative for all other treatment days. Second, the directional gradient field of the images from the training set sampled on the bladder vertices was assumed to be similar to the directional gradient field of the online localization image sampled on the bladder segmentation vertices.

The inputs of the segmentation method includes the CBCT image to be segmented, 5 CBCT images used in model building, 5 re-sampled 3D bladder contours corresponding to the five CBCT images, and several dominating PCA modes derived from the first 6 bladder contours.

One of the 5 CBCT image was chosen as the reference CBCT image. In order to suppress noise, a 3D recursive Gaussian smoothing filter [124] with standard deviation 3 mm was applied to both reference and validation CBCT images (figure 5.2). The re-sampled 3D bladder contour corresponding to the reference CBCT image was considered as the reference bladder contour  $c_0$ . For the purpose of calculating directional gradients, extra interior and exterior bladder contours  $c_{int}$  and  $c_{ext}$  were created by shrinking and expanding the vertices of reference bladder contour  $c_0$  by 5 mm along a direction normal to each vertex. The 3D contours  $c_0$ ,  $c_{int}$  and  $c_{ext}$  all had  $L$  ( $L=2091$ ) vertices and same triangular surface connections.

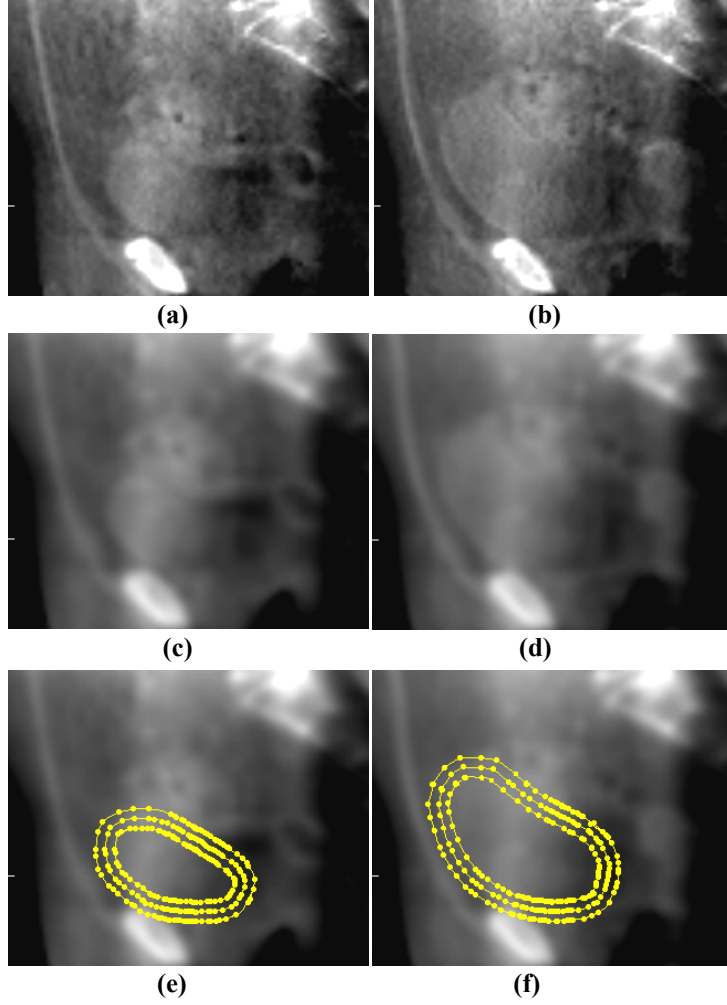


**Figure 5.2: Example of pre-processing of CBCT images and contours (Patient 5). The original reference CBCT image (a) and online CBCT image (b). After applying a Gaussian smoothing filter, (a) and (b) were converted to (c) and (d), respectively. In (e), the reference bladder contour with extra interior and exterior layers was overlaid on (c). The reference bladder contour was used as the initial segmentation and then deformed to fit the edge of bladder on online CBCT. In (f), the segmented bladder with extra interior and exterior layers was overlaid on (d).**

The bladder segmentation contour  $c_0^*(P)$  on the validation image started from the reference bladder contour  $c_0$ , where  $c_0^*(\{P_i = 0\}_{i=1,\dots,D}) = c_0$ . When changing the shape parameters vector  $\{P_i\}_{i=1,\dots,D}$ , which contains the weights of the principal PCA modes  $M$ ,  $\{M_i = q_i\}_{i=1,\dots,D}$ , the initial bladder contour would deform according to the deformation pattern calculated from the training dataset.

$$c_0^*(P) = c_0 + M \cdot P \quad (5.7)$$

Similarly, interior contour candidate  $c_{int}^*(P)$  and exterior contour candidate  $c_{ext}^*(P)$  were also created by shrinking and expanding the vertices of contour candidate  $c_0^*(P)$  by 5 mm along a direction normal to each vertex.

A cost function  $E$  was defined to measure how well the deformed bladder surface matched the underlying bladder edge on the validation image, based the absolute difference between the directional gradient of the reference CBCT sampled on its corresponding bladder contour and the directional gradient of the validation CBCT sampled on the segmentation contour candidate. The cost function was evaluated on the interior, central and exterior contours to capture information of the neighborhood of the bladder edge

$$E = \sum_{j=1}^L \left( \left| (I_R(\mathbf{c}_{0,j}) - I_R(\mathbf{c}_{\text{int},j})) - (I_V(\mathbf{c}_{0,j}^*(\mathbf{P})) - I_V(\mathbf{c}_{\text{int},j}^*(\mathbf{P}))) \right| \right. \\ \left. + \left| (I_R(\mathbf{c}_{0,j}) - I_R(\mathbf{c}_{\text{ext},j})) - (I_V(\mathbf{c}_{0,j}^*(\mathbf{P})) - I_V(\mathbf{c}_{\text{ext},j}^*(\mathbf{P}))) \right| \right) \quad (5.8)$$

where  $I_R(\mathbf{c})$  and  $I_V(\mathbf{c})$  notate the intensity of the reference image and validation image sampled by the vertex of contour  $\mathbf{c}$ .  $(I_R(\mathbf{c}_{0,j}) - I_R(\mathbf{c}_{\text{int},j}))$  and  $(I_R(\mathbf{c}_{0,j}) - I_R(\mathbf{c}_{\text{ext},j}))$  are the interior and exterior directional gradient values on the  $j$ th vertex of the reference bladder contour.  $(I_V(\mathbf{c}_{0,j}^*(\mathbf{P})) - I_V(\mathbf{c}_{\text{int},j}^*(\mathbf{P})))$  and  $(I_V(\mathbf{c}_{0,j}^*(\mathbf{P})) - I_V(\mathbf{c}_{\text{ext},j}^*(\mathbf{P})))$  are the interior and exterior directional gradients on the  $j$ th vertex of the segmentation contour.

The problem with identifying bladder boundaries was to find the optimum shape parameter vector  $\mathbf{P}^*$  that best represents the bladder surface in a validation image.

$$\mathbf{P}^* = \arg \min(E | \mathbf{P}) \quad \mathbf{P}_i \in [-3.1\sigma_i, 3.1\sigma_i] \quad (5.9)$$

$\sigma_i$  is the square root of the eigen value  $\lambda_i$ . The search for the optimum shape parameter vector  $\mathbf{P}^*$  was carried out by a simplex optimizer within the interval  $[-3.1\sigma, 3.1\sigma]$  to minimize the cost function of  $E$ .  $3.1\sigma$  is sufficient to cover 95% confidence interval up to 4 dimensional variates [125].

For each online CBCT image, the segmentations were done five times using a different reference CBCT image from the training dataset. The one with the lowest cost function was selected as the final bladder segmentation.

### 5.3.3 Validation

To evaluate the performance of the automatic bladder segmentation, we calculated the volume and distance based errors and accuracy of plan selection from library of plans using automatic bladder segmentation.

For the purpose of comparison, we used the conformity index (CI) to measure the volume overlap between the automatic and manual segmented bladders. For two regions  $R_1$  and  $R_2$ , the CI was defined as the ratio of the volume of intersection to volume of union between  $R_1$  and  $R_2$

$$CI(R_1, R_2) = \frac{\text{Volume}(R_1 \cap R_2)}{\text{Volume}(R_1 \cup R_2)} \quad (5.10)$$

The signed local residual error was defined by computing the distance of the position in manually delineated bladder surface to the triangles in automatic segmented

bladder surface. The residual was positive when the point from the manually delineated bladder surface was located outside the automatically segmented bladder and negative when the point from the manually delineated bladder surface was located inside the automatically segmented bladder. Note that the manual delineated bladder used for volume and distance based metrics calculation is the smoothed bladder delineation described before.

Besides the volume and distance based conformity test, the accuracy of plan selection using automatic segmentation was also calculated. Since the bladder shape is highly correlated with the bladder volume, for each patient, three plans with different PTV volume were created from the CTVs (bladder) in the first six scans, according to the protocol proposed by Foroudi et al. [54]. The small PTV was the smallest bladder of the six bladders with additional 5 mm uniform margin. The large PTV was the Boolean addition of all the six bladders with additional 5 mm uniform margin. In literature [54], the medium PTV was visually determined for each axial slice, from the largest and smallest bladders, using a ruler tool as a guide. However, in our study, for the sake of simplicity and reproducibility, instead of the visually determined contour the medium PTV was defined by the Boolean addition of the smallest  $F$  bladders out of the six bladders with additional 5 mm uniform margin.  $F$  was chosen such that the  $F$ th smallest bladder has the closest volume to the median volume of the largest and smallest bladders.

To study the segmentation accuracy needed for plan selection, we measured the variations between different sizes of PTV, i.e. the mean surface distance between small PTV to medium PTV, medium PTV to large PTV, and small PTV to large PTV. These variations between different sizes of PTV were compared with the segmentation errors.

For each validation CBCT scan, the best available plan from the library of plans was selected as the plan of the day from the three plans such that the plan for the smallest PTV could safely cover more than 99% of the bladder volume. We separately used the manually delineated and automatically segmented bladders to select the best available plan. There were four possible cases: either the plan for small, medium or large size PTV was selected or none of the three plans was sufficient to cover 99% of the bladder volume. We considered the plan selected using the manually delineated bladder as the reference. The agreement between the PTV size of the plan selected by the automatically segmented bladders and reference was recorded.

## 5.4 Results

The numbers of eigenmodes needed to represent the training data with less than 1 mm average residual errors are illustrated in figure 5.3. In general, two to four eigenmodes were needed for the 23 patients and this numbers of eigenmodes was used in the bladder segmentation procedure. Figure 5.4 visualizes the first three dominating eigenmodes of Patient 5. In the first eigenmodes, the bladder deformation is highly associated with bladder volume change. The second and third eigenmodes model translation and rotation of the bladder.

Figure 5.5 shows an example of five segmentation candidates, a final bladder segmentation, a manually delineated bladder, and three different PTVs from a library of plans. The averaged absolute residual error distribution over all 152 bladder segmentations illustrates a higher segmentation residual error in the cranial and posterior parts of the bladder (figure 5.6).

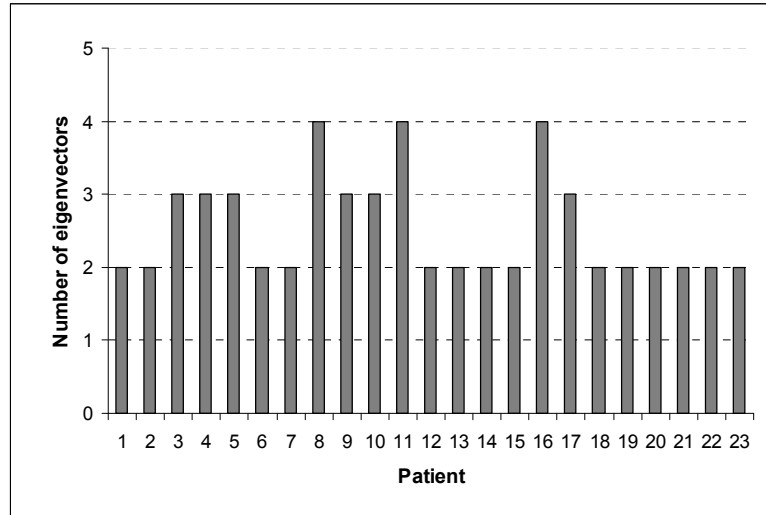


Figure 5.3: The number of eigenvectors needed to represent the bladder shapes of the training data with less than 0.1 cm mean absolute residual error for the 23 patients.

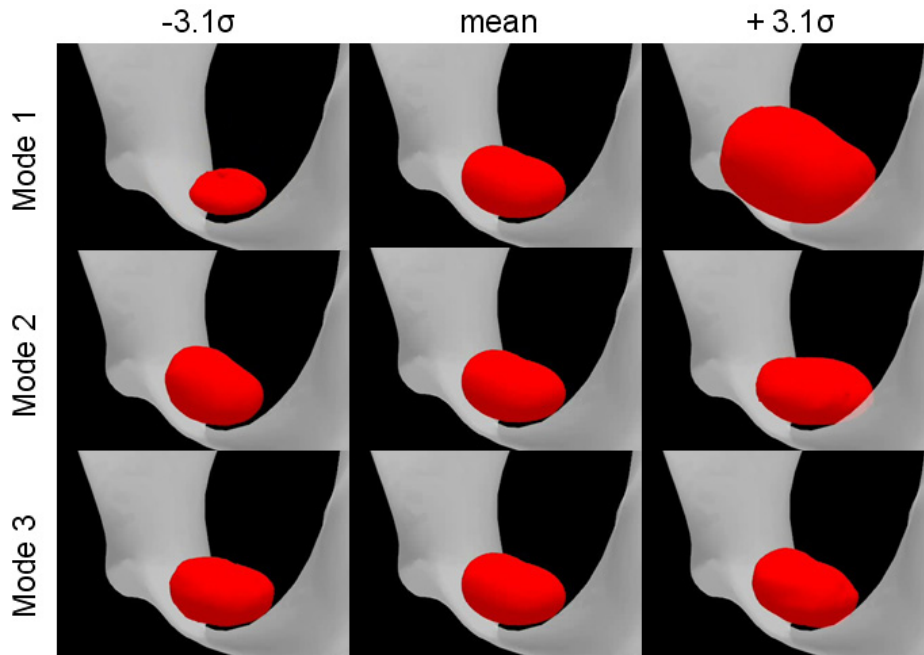
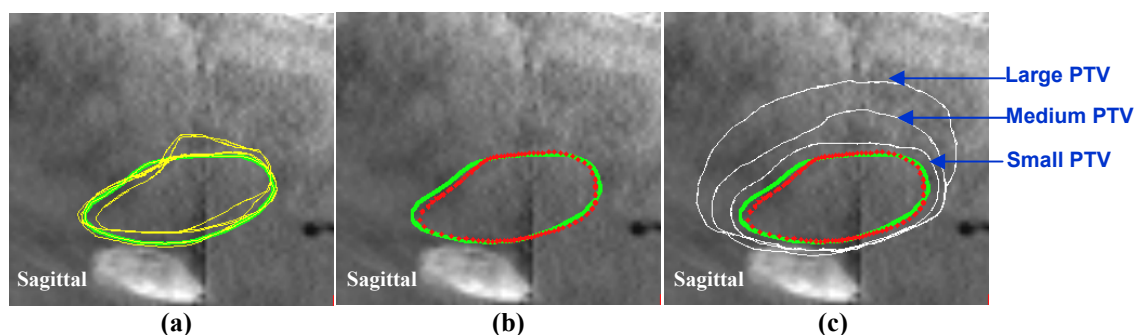
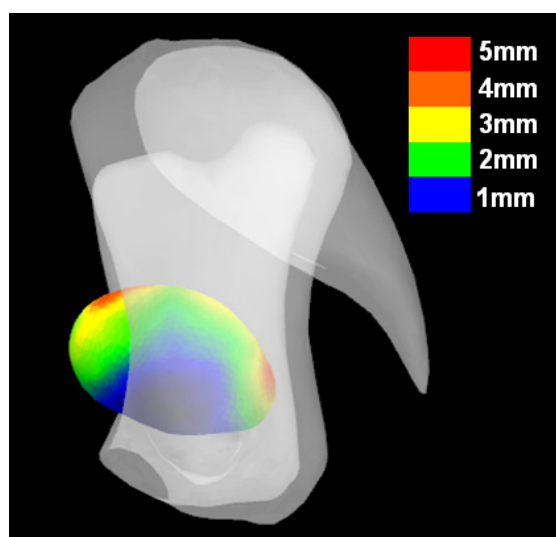


Figure 5.4: Illustration of the first three dominating eigenmodes of bladder shape variation of patient 5. The central column gives a 3D views of the mean bladder shape of the training data set, whereas the left and right columns give minus and plus 3.1 times the bladder shape variance relative to the mean shape. The white surface around the bladder is the pelvic bone.



**Figure 5.5 (a):** Five bladder segmentations (yellow thin solid curves) using different references were overlaid on a sagittal section of a validation CBCT image of Patient 6. The one with lowest cost function (green thick solid curve) was chosen as the final segmentation contour. **(b):** Comparison of the automatically segmented bladder contour (green thick solid curve) and manually delineated bladder contour (red dotted line) **(c):** Small, medium and large PTVs (white thin white curves) from the library of plans. In this example, the plan for the small PTV was selected as the plan of the day, since it was the smallest PTV safely covering more than 99% bladder volume.



**Figure 5.6:** Visualization of the global average residual error distribution over all 152 bladder segmentations.

The median, 10th percentile and 90th percentile of CI and SD of signed local residual error between manually delineated and automatically segmented bladders for each patient are plotted in figure 5.7 and figure 5.8. The global mean CI overlap indices and SD of signed local residual error over all 152 bladder segmentations from 23 patients are 78.5%, and 0.244 cm, respectively.

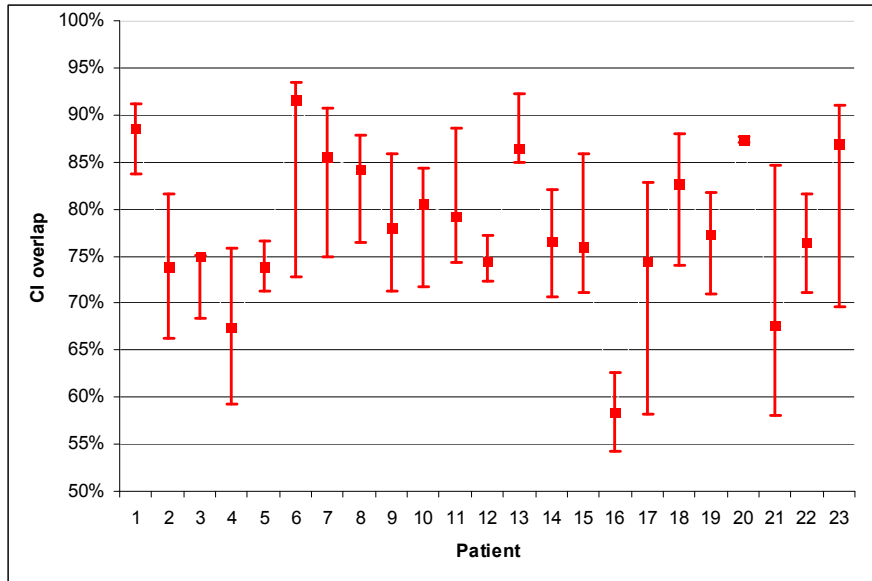


Figure 5.7: The median (solid square), and 10<sup>th</sup> percentile and 90<sup>th</sup> percentile (error bars) of the CI overlap between manually delineated bladder and automatically segmented bladder for 23 patients.

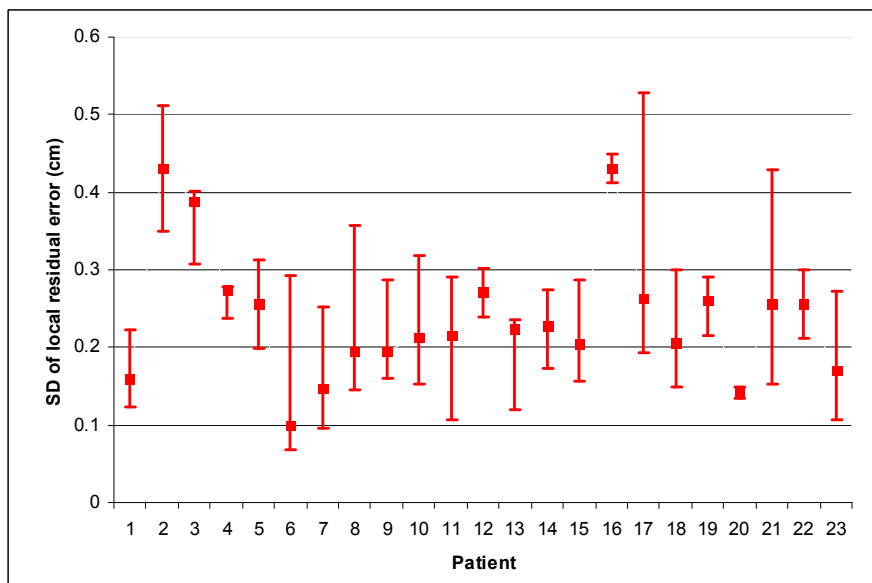


Figure 5.8: The median (solid square), and 10<sup>th</sup> and 90<sup>th</sup> percentile (error bars) of the standard deviation of signed local residual error between manually delineated bladder and automatically segmented bladder for 23 patients.

The mean and SD of the volume difference of automatic and manual bladder segmentation are -9.8 ml and 37.7 ml. Since the volume difference is so small, the mean signed residual errors over all 23 patients is almost zero (<0.03 cm).

The mean volume of the 14 patients with full bladder drinking protocol is 245.0 ml (range from 93.6 ml to 987.8 ml), while the mean bladder volume of the 9 patients with empty bladder protocol is 115.5 ml (range from 22.7 ml to 193.4 ml). We did not find a significant difference in distance based residual errors between full and empty bladders: mean residual error 0.247 cm for full bladder and mean residual error 0.242

cm for empty bladder ( $p > 0.5$ , paired t-test). Since overlap index is very sensitive to bladder volume, the CI overlap index for full bladder is significantly higher than that for empty bladder ( $p < 0.01$ , paired t-test). The mean CI overlap indices for full and empty bladder are 80.3% and 75.2%, respectively.

The number of plans for small PTV, medium PTV and large PTV chosen by manually delineated bladder for each patient is plotted in figure 5.9. Pooling all patients together, the plans with small, medium and large PTV were selected in 39.5%, 34.9% and 17.8% of the cases, respectively. In the remaining 7.9% of cases, none of the three plans was sufficient to fully cover the target.

The mean surface distances between the small and medium PTVs, medium and large PTVs and small and large PTVs are 0.339 cm, 0.317 cm and 0.607 cm, respectively.

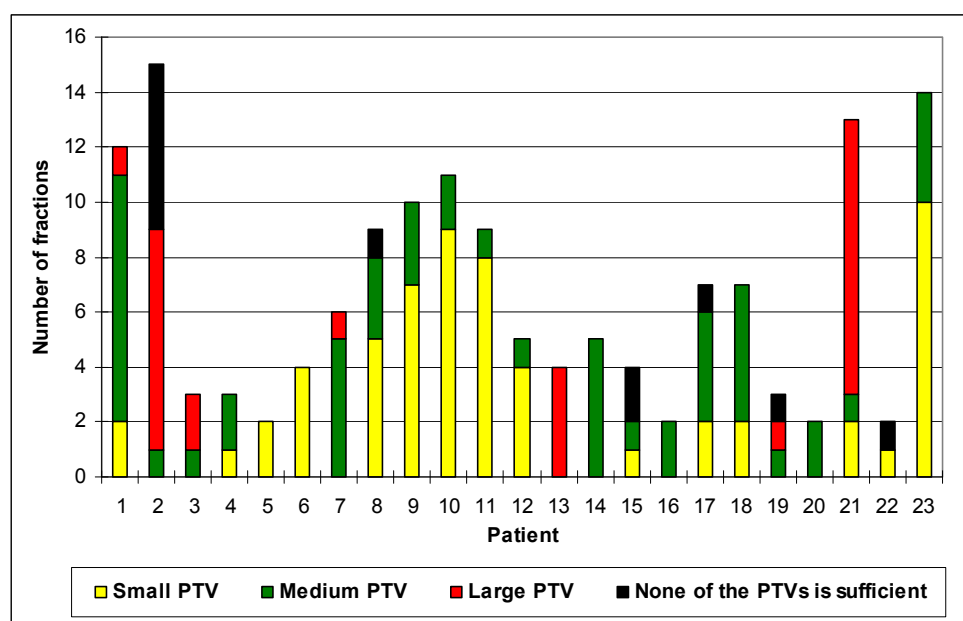


**Figure 5.9:** Plan selection frequencies (the times of the plans with small, medium and large PTV were selected and the times of none of the PTVs was sufficient to cover the target) for each patient chosen by manually delineated bladder.

The agreement between the selections made by automatic and manual bladder segmentations is 77.6% (figure 5.10). In 15.8% of the cases, the plan selected by automatic segmentation is one size larger or smaller than the plan selected by manual segmentation. In 6.6% of the cases, the plan selected by automatic segmentation is two sizes larger or smaller than the plan selected by manual segmentation.

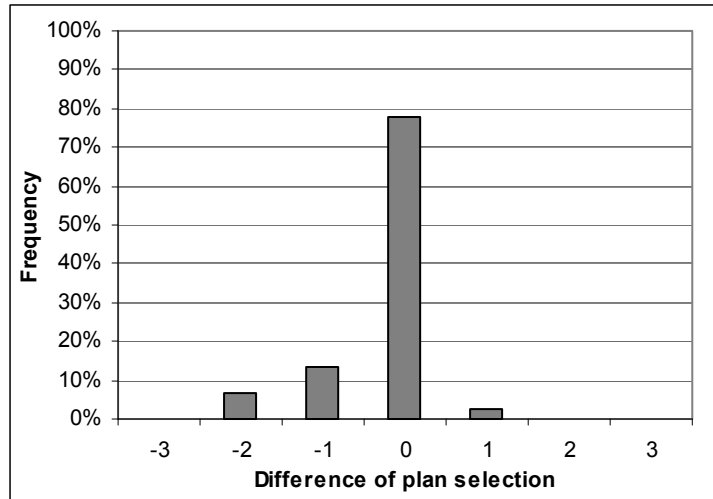


**Figure 5.10:** Histogram of the difference between the plans selected by manual and automatic bladder segmentation. The zero position in on the horizontal axis is where plans selected by manual and automatic segmentations correspond. The other non-zero numbers in x axis indicate difference of plan size selected by manual and automatic segmentations, e.g. when a plan for the large PTV was selected by manual segmentation, while a plan for the medium PTV was selected by automatic segmentation, the difference of plan selection was -1.

The total automatic segmentation and plan selection time for each CBCT image is less than 30 seconds on a personal computer equipped with Intel Core 2 Duo CPU of 3.0 GHz and 4 GB of RAM.

## 5.5 Discussion

We have presented a novel method of bladder segmentation based on patient-specific information and tested it on a large amount of CBCT images. Using individual bladder deformation patterns acquired early during treatment, this method is robust to handle the relatively poor image quality of CBCT and can produce reliable bladder segmentation in a short time. This segmentation method can achieve an accuracy of 78.5% mean CI overlap between manually and automatically segmented bladder, which is similar to the inter-observer variability of bladder delineation on CBCT reported in literatures, which are 75.0% CI overlap from Foroudi et al. [126] and 82% from Lutgendorf-Caucig et al. [127].

One assumption of this segmentation method is that in bladder motion, each voxel on the bladder wall always moves along the radial direction, hence, when there is bladder volume difference between the reference and validation images, the gradient value of a bladder contour vertex of the reference image is the same as the gradient value of the corresponding bladder contour vertex of the validation image. However, this correspondence defined along the radial direction is not necessarily anatomically true, especially when a large deformation or shifting occurs. Sometimes, even though the correspondence is anatomically right, the gradient values on the corresponding vertices between the reference and validation images could be largely different due to image artifacts. So, when there is a large difference of bladder volume between the

reference and validation images or a strong artifact in the reference image, the segmentation has a higher chance of failure. To deal with these problems, we used five separate CBCT images and its bladder contour as reference images and initial segmentations to segment the bladder on validation image. The segmentation with lowest cost function was selected as the final result. When the reference image has similar bladder volume as the validation image, it is more likely that the correspondence is anatomically true and validation image has same artifact as the reference image. Usually the reference image with the closest bladder volume to the validation image yielded the lowest cost function. This multiple reference strategy efficiently avoids segmentation failure caused by under-defined correspondence, image artifacts and local minima.

The other assumption of this segmentation method is that the PCA modes of bladder shape variation calculated from the first six scans are representative of other treatment days, whereas the CBCT images acquired in later stage of treatment could show different bladder shapes than the first six scans. The difference in bladder shape could be caused by differences in rectal and small bowel filling that were not present during the early stage. We believe this is the reason why the cranial-anterior region and posterior region, which are close to small bowel and rectum, have larger residual segmentation error than other regions (figure 5.6). In 12 out of 152 validation CBCT images, the automatic bladder segmentation has low similarity with the manual delineation (CI overlap < 65%). These 12 failed cases were from 4 patients, which partially explains the large variation of the error bars in figure 5.7. In these 12 failed cases, we found that due to extreme rectum and bladder fillings, the real bladder shapes deviate largely from the first six bladders. This is a limitation of any method based on a patient-specific model. In practice, a visual check of the quality of segmentation will therefore always be part of the procedure. When a failed segmentation is found, for instance the largest plan can be selected. To improve the patient-specific model, we did some extra analysis, that when segmentation was performed to each online CBCT, all the available previous CBCT scans were included to update the training model. Such model including every successive CBCT improved the average CI overlap to 80.8%. However, this model requires considerable amount of extra labor and is therefore unlikely to be implemented in practice. To avoid the limitation of the patient-specific model, we are currently investigating the bladder segmentation method only using a population based PCA model and planning CT image as input. The preliminary results show that the average CI overlap of automatic bladder segmentation using a population based model is 70.5%. The main reason why population based models yield worse segmentation results than patient-specific models is that non-global optimized cost functions were often found due to the low similarity between bladder borders on planning CT and online CBCT.

All the bladder contours were delineated slice-by-slice and then connected to a 3D surface mesh. A simple smoothing filter was applied to remove the spikes between different slices. A problem of such linear smoothing filter was that a scaling was required to compensate the volume shrinkage caused by the smoothing filter and this compensation could result in some shape distortion. We measured that the mean absolute surface distance between original and smoothed contours was 0.4 mm, i.e. the shape distortion caused by smoothing was very limited. Taubin [128] developed a smoothing filter that using two diffusion steps, one inwards and one outwards to

attenuate details while keeping the surface in roughly the same position. This is a possible way to reduce the shape distortion resulted by the smoothing in current study.

In the segmentation process, a 3D Gaussian smoothing filter with SD of 3 mm was applied to both the reference and validation images. The size of the smoothing filter was chosen by a parameter optimization test. When the segmentation method was performed on the CBCT image with Gaussian smoothing filter with SD of 0 mm, 1 mm, 2 mm, 3 mm, 4 mm and 5 mm, the overall mean CI overlap was 69.2%, 74.9% , 77.9%, 78.5% ,77.6% and 75.5%, respectively. This data shows that the size of the filter only had a small effect on the segmentation results. In this study, 3 mm was chosen as this yielded the highest CI overlap.

We calculated the summation of absolute interior and exterior directional gradients as the cost function in equation (5.8). The distance between the interior, central and exterior bladder contours to calculate the directional gradients is related to the size of smoothing filter. For the Gaussian smoothing filter with SD of 3 mm, a parameter testing shows that 5 mm distance to calculate the interior and exterior directional gradients relative to the central bladder contour gave the best results. Only using two layers, the interior and exterior contours, to compute the gradient field would be a simpler expression of the cost function. The latter achieves an average CI of 78.2%, which is slightly lower than that of using the cost function with three layers. However, using more than three layers did not improve the results.

Several groups reported that the multiple plan adaptive strategies can better spare the organs at risk than traditional radiotherapy [22;23;29;55-58], and our study has the consistent finding as these groups. The mean bladder volume, i.e. CTV volume, of the 152 CBCT used in our study is 211.1 ml. The traditional plan with 15 mm margin can safely cover the target (>99% volume coverage) in 88.8% cases, and the mean PTV volume is 619 ml. The multiple plan strategy safely covers the target in 92.1% cases with a mean PTV volume of only 316 ml. With online plan re-optimization, the PTV could be generated by the online segmented bladder plus a small margin. The online re-optimization strategy using the bladder segmentation plus a 5 mm margin as PTV can safely cover the target in 83.6% cases using a mean PTV of 283.6 ml. This comparison between the three strategies shows that the multiple plan strategy dramatically reduces radiation volume, however the additional benefit of plan re-optimization is very limited.

Two out of 43 patients were not selected in our study because of poor image quality of CBCT for manual delineation. The CBCT images of those 2 patients were mostly acquired very early (2004) when CBCT was just introduced for radiotherapy guidance. As CBCT imaging techniques have been developed, especially after the introduction of a bow-tie filter, the image quality of CBCT has improved. So, we believe our segmentation method will work better with recent CBCT systems.

From 2006, most patients in our department received a lipodol (liquid marker) injection on bladder wall via cystoscopy before planning, which was used for both tumor demarcation and image guidance [81;129]. However, the patients with lipiodol markers were excluded from our study. That is because the part of the bladder wall with markers has much higher gradient values than other parts, hence it dominates the cost function. When the markers do not move along the radial direction, it is very

likely to result in a wrong segmentation. In other words, the image data with lipiodol on bladder wall is not compatible with the current algorithm.

ART has emerged as an alternative to conventional RT. The multiple plan ART of bladder cancer is currently considered as the best way to achieve an optimal trade-off between tumor coverage and sparing of the surrounding normal tissues. However, multiple plan ART significantly increases the treatment time and technicians' workload. Our method can currently automatically segment bladder within 30 seconds, which is much faster than a manual plan selection (1.5 min) [23]. The convolution operation of Gaussian smoothing on five reference images requires 60% of computation time. This computation time can easily be reduced by optimizing the code, using parallel computing, or by simply pre-computing the data.

The agreement between selections made by manually delineated and automatically segmented bladders is 77.6%, which is slightly better than the reported agreement between different observers (range from 70% to 77% [23;55;116]). We may therefore conclude that our automatic segmentation provides a fast and robust plan selection tool that facilitates clinical implementation of multiple plan ART of bladder cancer.

In literature, there were various protocols used to generate multiple plans with different PTV volume. However, because of the intra-fractional bladder motion, the plan selection volume is always smaller than the real PTV [22;23;29;55;56;58]. Vestergaard et al. [22] and Foroudi et al. [58] used a region 3 mm smaller than PTV and 95% isodose line to select the plan of the day. In our study, the generated three PTV contours only take into account the inter-fractional bladder motion. According to our intra-fractional bladder filling study, in practice we recommend an extra 4 mm margin for empty bladder and 3 mm for full bladder to compensate for the 8 minutes' intra-fractional motion. Note that the size of the margin is highly correlated to treatment time. Fast radiation delivery techniques like VMAT can significantly reduce the treatment time and therefore reduce the intra-fractional safety margin.

## **5.6 Conclusion**

PCA is an efficient method to describe patient-specific bladder deformation. The statistical shape based segmentation approach is robust to handle the relatively poor CBCT image quality and allows for fast and reliable automatic segmentation of the bladder on CBCT. This automatic segmentation can be used to select the appropriate plan from a library of plans for a multiple plan ART of bladder cancer. However, manual delineation of the first five CBCT is required, which is time consuming.

### **Acknowledgement**

The authors would like to acknowledge Hermine Ribbers for her assistance of copying and selecting data.